Thin Single-Walled Carbon Nanotubes with Narrow Chirality Distribution: Constructive Interplay of Plasma and Gibbs–Thomson Effects

Kostya (Ken) Ostrikov[#,*] and Hamid Mehdipour[#]

Plasma Nanoscience Centre Australia (PNCA), CSIRO Materials Science and Engineering, P.O. Box 218, Lindfield, New South Wales 2070, Australia, and Plasma Nanoscience @ Complex Systems, School of Physics, University of Sydney, New South Wales 2006, Australia. [#]Both authors made equal contributions to this work.

ABSTRACT Multiscale, multiphase numerical modeling is used to explain the mechanisms of effective control of chirality distributions of single-walled carbon nanotubes in direct plasma growth and suggest effective approaches to further improvement. The model includes an unprecedented combination of the plasma sheath, ion/radical transport, species creation/loss, plasma–surface interaction, heat transfer, surface/bulk diffusion, graphene layer nucleation, and bending/lift-off modules. It is shown that the constructive interplay between the plasma and the Gibbs–Thomson effect can lead to the effective nucleation and lift-off of small graphene layers on small metal catalyst nanoparticles. As a result, much thinner nanotubes with narrower chirality distributions can nucleate at much lower process temperatures and pressures compared to thermal CVD. This approach is validated by a host of experimental results, substantially reduces the amounts of energy and atomic matter required for the nanotube growth, and can be extended to other nanoscale structures and materials systems, thereby nearing the ultimate goal of energy- and matter-efficient nanotechnology.

KEYWORDS: single-walled carbon nanotubes · plasma nanoscience · chirality control · graphene layer

Owing to their fascinating mechanical, electronic, chemical, and other properties, single-walled carbon nanotubes (SWCNTs) are presently among the most attractive building blocks of a variety of nanodevices for energy conversion and storage, environmental and biomedical sensing and imaging, drug delivery, bioscaffolding in regenerative medicine, gene, protein, and DNA targeting, cellular control, gas separation, water purification, and integrated nanoelectronic curcuitry, to mention just a few.[1–4] The response of SWCNTs in applications critically depends on the distributions of their lengths, thicknesses, and chiralities, which determine the properties of the nanotube arrays. Despite almost two decades of intense research, the problem of effective control of these parameters still remains unsolved and the as-grown nanotube arrays commonly contain a mix of thick and thin, semiconducting, and metallic nanotubes as well as a large variety of chiral structures. Sophisticated postsynthesis chemical separation protocols are required to separate the SWCNTs by their chirality and metallicity.[5] However, the problem of direct growth of very thin nanotubes with narrow size, diameter, and chirality distributions directly in the specified device locations and at device-tolerable process temperatures still remains.

Recent results suggest that this control can be improved by tailoring arrays of catalyst nanoparticles (*e.g.*, size/position uniformity, alloying/layering, and lattice space) and understanding atomic processes on catalyst surfaces with imperfections as well as the transient nucleation and relaxation dynamics.[6–8] This, mostly catalyst-related, approach is presently believed to be the most promising solution. However, very recent results on the effective plasma-based control of the SWCNT chirality and sizes[9–15] suggest that several other factors such as the process pressure and temperature, precursor gas composition, and the rates, duration, and selectivity of precursor supply strongly affect the distributions of the nanotube chirality and sizes on the same catalyst patterns.

This is why a clear understanding of the SWCNT nucleation mechanism in its entirety is required, including carbon species production, delivery to the catalyst, surface and vapor transport, energy/matter exchange processes, and catalyst supersaturation, followed by graphene layer nucleation and lift-off. Many techniques such as classical molecular dynamics (MD), Monte Carlo (MC), density functional theory (DFT), gas-phase species production, surface kinetic

* Address correspondence to kostya.ostrikov@csiro.au.

Received for review August 12, 2011 and accepted September 9, 2011.

Published online September 09, 2011
10.1021/nn2030989

models, and a variety of hybrid approaches are presently used to simulate separated aspects of this complex process that spans over multiple space and time scales. To remain within reasonable computational cost and reliability, the most advanced simulations rely on many tractable yet artificial assumptions about interatomic interaction potentials, as well as the numbers of atoms involved, time scales of various precursor–catalyst interactions, *etc.*, that in most cases are several orders of magnitude different from experimental reality.[8,16]

To avoid such problems and directly relate the numerical results to the experiments, here we use a multiscale, multiphase numerical model based on the plasma-produced building unit (BU) appoach.[17] This model allows a simpler yet interlinked and tractable description of the plasma sheath structure, ion/radical transport to the surface, and interaction of the plasma with the catalyst nanoparticle surface, which involves carbon/hydrogen species creation/loss and heat exchange. This description is coupled to the surface/bulk diffusion of carbon atoms on/in catalyst, followed by the graphene cap nucleation, bending, and lift-off.

Using this model, we show how to maximize the benefits from both plasma and Gibbs–Thompson (GT) effects and enable their constructive interplay to produce thinner SWCNTs with a narrow size/chirality distribution at process temperatures and pressures that are substantially lower than in thermal chemical vapor deposition (CVD). The GT effect, which is commonly known as a reduction of supersaturation with decreasing the size of the growth seeds, leads to higher rates of extrusion of precursor atoms as catalyst nanoparticles get smaller.[18,19] This increases the nanostructure nucleation barrier, thus demanding higher process temperatures (which in the case of very thin SWCNTs commonly reach 800–900 °C and even higher) and pressures to compensate for the diminished catalyst supersaturation levels.

Our results suggest that the GT effect impacts both positively and negatively on the SWCNT growth. More importantly, the plasma effects are shown to maximize the positive GT impact by a stronger bending and lifting of the graphene layer to form a nanotube cap. The plasma–surface interactions also minimize the negative impact of the GT effect by substantially reducing the SWCNT nucleation temperature and pressure and enabling a better size selectivity at lower temperatures on small catalyst nanoparticles. The results of our numerical modeling are consistent with a host of experimental observations on thermal and plasma synthesis of SWCNTs. In particular, they explain the key results of the very recent experiments on the effective plasma-based control of the SWCNT chirality and sizes[9–14] and provide suggestions for the further improvement of this ability.

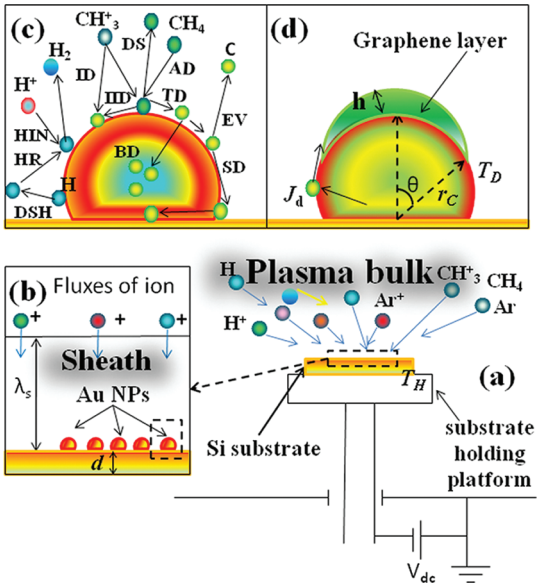

Figure 1. Plasma–surface interactions involved in the nucleation and growth of single-walled carbon nanotubes in reactive Ar+H_2+CH_4 plasmas: (a) substrate heating and species deposition; (b) plasma sheath and Au CNPs on a Si substrate; (c) plasma-related processes on the Au CNP surface; (d) CNP saturation, carbon atom extrusion, and GL nucleation. The most important surface processes involved in carbon atom production and catalyst nanoparticle heating are ion-induced dissociation (IID), ion decomposition (ID), hydrogen recombination (HR), ion-induced neutralization (HIN), adsorption of hydrogen atoms (ADH), desorption of hydrogen atoms (DSH), adsorption (AD) and desorption (DS) of hydrocarbon radicals, evaporation (EV), bulk (BD) and surface diffusion (SD) of carbon atoms, and thermal dissociation of hydrocarbon radicals (TD).

RESULTS AND DISCUSSION

Plasma and Gibbs–Thompson Effects in SWCNT Nucleation. We consider the Au catalyst nanoparticle (CNP)-assisted nucleation of a SWCNT in reactive plasmas of Ar + H_2 + CH_4 gas mixtures commonly used in plasma-aided synthesis of carbon nanotubes.[20] Figure 1 shows a large variety of elementary acts of plasma–surface interactions involved in this process. The primary step in the SWCNT formation is the formation of a graphene layer (GL) on the top surface of the catalyst nanoparticle. This is strongly (and positively) affected by the GT effect of an increase in carbon atom concentration in small CNPs and more effective carbon precipitation on the surface of the Au nanoparticle rather than on the CNP–substrate interface. If the kinetic energy (per area), E_K, associated with the coordinated detachment of the carbon atoms from the CNP surface is higher than the work of adhesion (per area), W_{ad}, of the as-nucleated graphene layer to the nanoparticle surface, the GL bending takes place as sketched in Figure 1d.[21] Furthermore, if the number of atoms in the GL satisfies the isolated pentagon rule,[22] a stable cap is formed, giving rise to the specific SWCNT chirality. The continuously created carbon atoms precipitate from the surface and bulk of the nanoparticles and incorporate into the nanotube wall through the open reactive edges, thus enabling the SWCNT growth.

As the nanoparticles get smaller, the GT effect leads to the faster catalyst saturation and loss of carbon atoms before the nucleation process on the outer surface is complete. In addition, the minimum radius of a stable GL also increases due to the GT effect. This in turn results in higher nanotube nucleation barriers ΔG_N^*, which is a negative impact of the GT effect. To compensate for this loss and enable faster nucleation, higher precursor pressures and surface temperatures are required in thermal CVD. This also leads to the decreased stability of small catalyst nanoparticles (*e.g.*, coagulation into larger particles). The driving force for carbon precipitation on the catalyst surface is determined by the difference $\Delta\mu_{ls}$ in chemical potentials in the liquid (nanoparticle) and solid (GL) phases. This difference decreases at lower surface temperatures and smaller catalyst radii. Hence, nucleation of thin SWCNTs on small nanoparticles is very difficult, if possible at all, at low temperatures. It is also not possible on larger nanoparticles, as they are expected to have larger minimum radii of stable GL nuclei and also a larger work of adhesion (per area).[23] In this case, the surface temperature becomes insufficient for the GL bending, thereby leading to the formation of carbon nanocages or other nanostructures.[24,25] The above driving force in turn determines the kinetics of the nucleation and growth of carbon nanotubes starting from small graphitic nuclei (such as the GL nuclei in our case), which in most cases proceeds under far-from-equilibrium conditions.[26]

Our strategy in this work is based on using plasma-specific effects to maximize the positive impact while minimizing the negative impact of the GT effect in the nucleation of thin SWCNTs on small CNPs at low process temperatures and pressures and also increasing the size selectivity of this process. On one hand, effective carbon atom production through highly reactive plasma chemistry enhanced by electron- and ion-assisted dissociation and faster delivery of ionic species make it possible to compensate for the loss of carbon atoms and significantly reduce the nucleation barrier (thus minimizing the negative impact) associated with the GT effect. On the other hand, localized heating of the nanoparticles through the plasma-specific heat exchange on the CNP surface enhances GL nucleation through the enhanced surface and bulk diffusion of carbon atoms. In this case, carbon atoms are also energized, which increases their kinetic energy and hence the GL bending energy. Furthermore, since the work of adhesion also decreases as the catalyst nanoparticles get smaller, this also leads to the narrower size (and hence, chirality) distribution of the SWCNT on smaller CNPs. The better selectivity in this case is due to the larger differences between the nucleation barriers and bending energies of different-chirality nanotubes compared to thermal CVD. This further improves the tendency toward selective nucleation of thinner SWCNTs with a narrower chirality distribution in the plasma, at lower substrate temperatures.

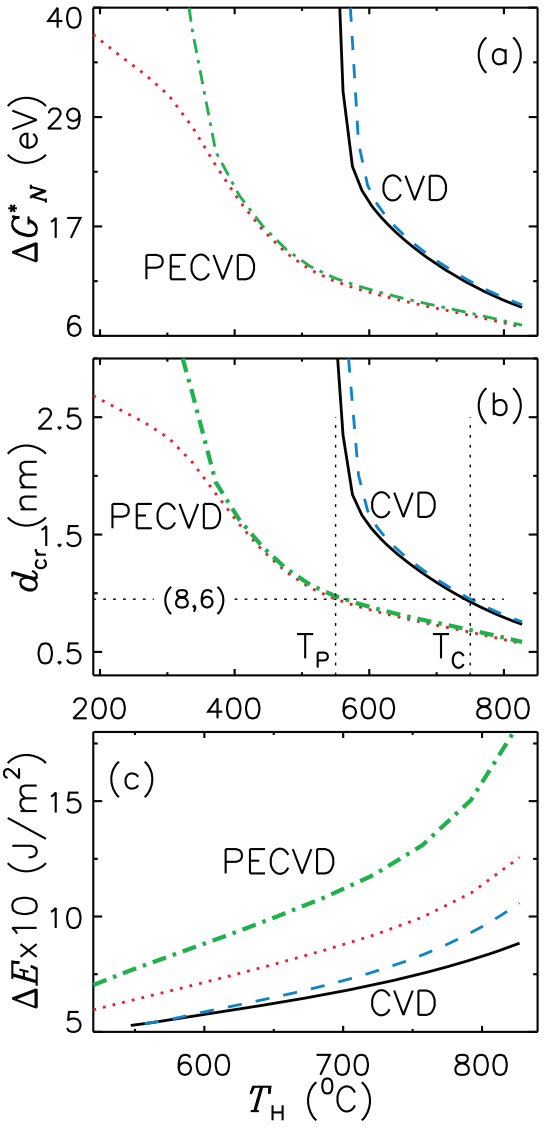

Figure 2. Energy barrier for GL nucleation (a), critical diameter (b), and bending energy (c) as functions of the substrate holder temperature for CVD (solid and dashed curves) and PECVD (dotted and dash−dotted curves) for electron temperature T_e = 2.0 eV, ion temperature T_i = 0.05 eV, plasma density $n_{e0} = 5.0 \times 10^{12}$ cm^{-3}, gas pressure P_0 = 50 mTorr, Au CNP radius r_C = 2.0 nm, surface potential $\Phi_S = -100$ V, and relative abundances r_{Ar} = 70%, r_{CH} = 20%, and r_H = 10% of Ar, CH_4, and H_2 in the gas mixture. The dashed and dash−dotted curves take the GT effect into account. T_C and T_P are the temperatures for the nucleation of a (8,6) semiconducting SWCNT[11] in CVD and PECVD, respectively.

Numerical Results and Experimental Support. Here we present the results of our numerical calculations that support the above approach. Relevant experimental results that further validate our approach are also discussed. Further details about the model, elementary processes considered, and assumptions made can be found in the Methods section and in the Supporting Information.

Graphene Layer: Lower Barriers and Temperatures, Smaller Nuclei, and Stronger Bending. The results in

Figure 2 are related to the first step of the SWCNT growth, namely, the nucleation and then bending of a critical graphene nucleus of diameter d_{cr} on top of a Au catalyst nanoparticle of radius r_c (Figure 1d). Figure 2a–c shows the dependence of the energy barrier for GL nucleation, ΔG_N^*, the critical diameter, and the work of bending $\Delta E = E_K - W_{ad}$ on the external substrate heating temperature T_H in a neutral gas chemical vapor deposition and plasma-enhanced CVD (PECVD) at the same precursor gas composition, operating pressure, and external heating conditions. Plasma-surface interactions (*e.g.*, hydrogen recombination and ion bombardment) lead to additional catalyst surface activation and heating.[27,28] These interactions also produce larger amounts of carbon atoms through gas-phase and surface dissociation of hydrocarbon precursors. This also enhances surface and bulk diffusion and, hence, catalyst supersaturation, and eventually the driving force $\Delta\mu_{sl}$ for the GL nucleation, which is the difference between the chemical potentials inside and on the surface of the catalyst nanoparticle. This leads to several important conclusions that are evident from Figure 2 and are supported by numerous experimental reports.

First, the barriers for GL nucleation and the sizes of the stable nuclei are significantly lower in the PECVD. Indeed, at T_H = 600 °C, ΔG_N^* is ~2.3 times lower and d_{cr} is ~1.5 times smaller than in thermal CVD. Hence, much smaller, stable graphene nuclei are possible in the plasma at much lower substrate temperatures. No stable GL nucleation may be expected in a thermal process below ~530 °C, whereas in the plasma the GL nucleation may take place even at external heating temperatures as low as ~200 °C. The minimum T_H to nucleate a GL required to produce an (8,6) single-walled nanotube (which showed a very strong abundance in recent plasma-based SWCNT synthesis[11]) is at least 750 °C in thermal CVD, while only 540 °C would be sufficient while using the plasma (Figure 2b).

Second, the bending energy, which is essential to form a SWCNT out of a graphene nucleus, may be substantially increased in the plasma, as can be seen in Figure 2c. This increase can be made much stronger through the positive effect of the GT mechanism. Moreover, this positive effect is stronger in the PECVD, thus evidencing a positive interplay of the plasma and GT effects. Indeed, at T_H = 600 °C, the GT effect alone almost does not increase ΔE in the CVD, while in the plasma it boosts the GL bending energy by about 30%, thereby increasing the overall gain over the thermal process to almost 60% (Figure 2c).

However, care should be taken so as not to reduce external heating below a certain threshold below which the formation of other carbon nanostructures (*e.g.*, graphene nanodots or carbon nanocages encapsulating the whole catalyst nanoparticle) would become more

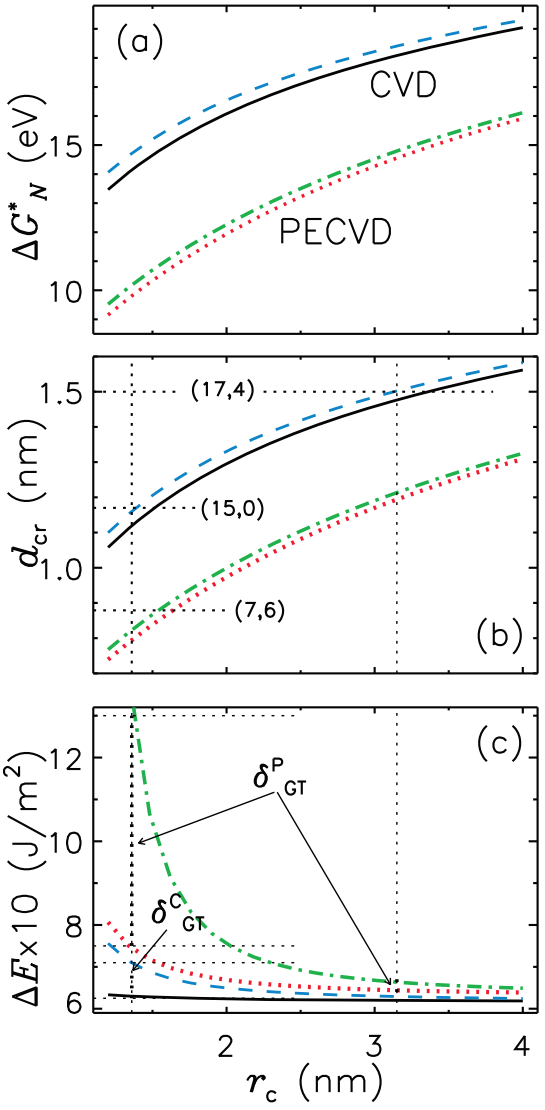

Figure 3. Energy barrier for GL nucleation (a), critical diameter (b), and bending energy (c) as functions of the CNP radius for CVD (solid and dashed curves) and PECVD (dotted and dash–dotted curves) for T_H = 650 °C and n_{e0} = 1.0 × 10^{12} cm^{-3} and all other parameters the same as in Figure 2. The dashed and dash–dotted curves take the GT effect into account. Examples of thin (7,6)[6,10,11] and thick (17,4) semiconducting and (15,0) metallic nanotubes are shown. δ_{GT}^C and δ_{GT}^P denote the gains in bending energy due to the GT effect in CVD and PECVD, respectively.

favorable. Indeed, below 380 °C, much larger GLs nucleate (Figure 2b), after overcoming much higher energy barriers (Figure 2a). Since the bending energy is significantly lower (Figure 2c) than at higher temperatures (the kinetic energy of carbon atoms E_K increases as the nanoparticle gets hotter, hence the bending energy ΔE also increases), the larger GLs will stay stuck to the catalyst surface, thus forming nanocage-like structures rather than single-walled nanotubes, which is consistent with the experimental reports by other authors.[24,25] Thus, thin SWCNTs are more probable at relatively higher temperatures, which is confirmed by the experimental reports on temperature dependence of SWCNT

nucleation and growth.[29−31] The decrease of the SWCNT nucleation temperatures by more than 200 degrees in PECVD (Figure 2) is supported by numerous recent experiments.[9−13,32−34]

Nucleation and Bending: Smaller Catalyst−Thinner, Size-Selected Tubes. Figure 3 shows how the effective interplay of the plasma and GT effects leads to the nucleation of thinner SWCNTs on smaller catalyst nanoparticles, with a better size selectivity compared to thermal CVD. First, the energy barriers for the GL nucleation are consistently lower (~50%) in the plasma over the entire range of catalyst radii considered (1−4 nm), as seen in Figure 3a. Second, a similar conclusion holds for the critical diameter of the stable nuclei, suggesting an even more significant (up to 60%) reduction in the plasma-based process (Figure 3b). For example, a Au catalyst nanoparticle with a radius of 1.36 nm may nucleate a large (15,0) nanotube in a purely thermal process, while a much thinner (7,6) nanotube may be possible in the plasma.

Third, the difference between the neutral gas- and plasma-based processes becomes more and more significant as the catalyst nanoparticles become smaller. Indeed, the difference between the GL bending energies in the two cases increases for smaller particles. More importantly, the GT effect makes this difference even more dramatic. Indeed, while ΔE^P is only 1.25 times larger than ΔE^C without accounting for the GT effect (superscripts P and C stand for PECVD and CVD cases, respectively), it becomes almost two times larger when the GT effect is taken into account (Figure 3c). In other words, bending of smaller GMLs on smaller catalyst nanoparticles is stronger in the plasma, eventually producing thinner single-walled carbon nanotubes. This conclusion is supported by the recent results suggesting that the (7,6) semiconducting chiral SWCNT is one of the most abundant nanotubes produced in recent experiments on SWCNT chirality control in the plasma,[6,11,12] while "hard-to-bend" thicker nanotubes such as the (15,0) zigzag metallic SWCNT are fairly rare in thermal CVD at the relatively low temperature of this example.

Fourth, the results in Figure 3 confirm better nanotube size selectivity in the plasma-based process. Indeed, the slopes of all plasma-related curves for the GL nucleation energy barrier (Figure 3a), critical diameter (Figure 3b), and bending energy (Figure 3c) are larger. This means that any two nanotubes with different radii (and hence, chiralities) will have larger differences in the energy and size thresholds for their nucleation in PECVD. This difference is larger at smaller catalyst sizes, as can be seen in Figure 3a, b. However, the most dramatic difference in the nanotube size selectivity materializes through the combined plasma and GT effects on the GL bending energy in the small catalyst nanoparticle size range below 2 nm (Figure 3c). In this size range, the dependence of ΔE on r_C is much steeper than for larger particles. Hence, the difference between the bending energies of any two selected nanotubes that nucleate on small catalyst nanoparticles becomes notably larger if both the plasma and the GT effects are taken into account. These trends explain the reported excellent selectivity of thin single-walled carbon nanotube growth on smaller catalyst nanoparticles in the plasma.[9−13] This selectivity was reported to

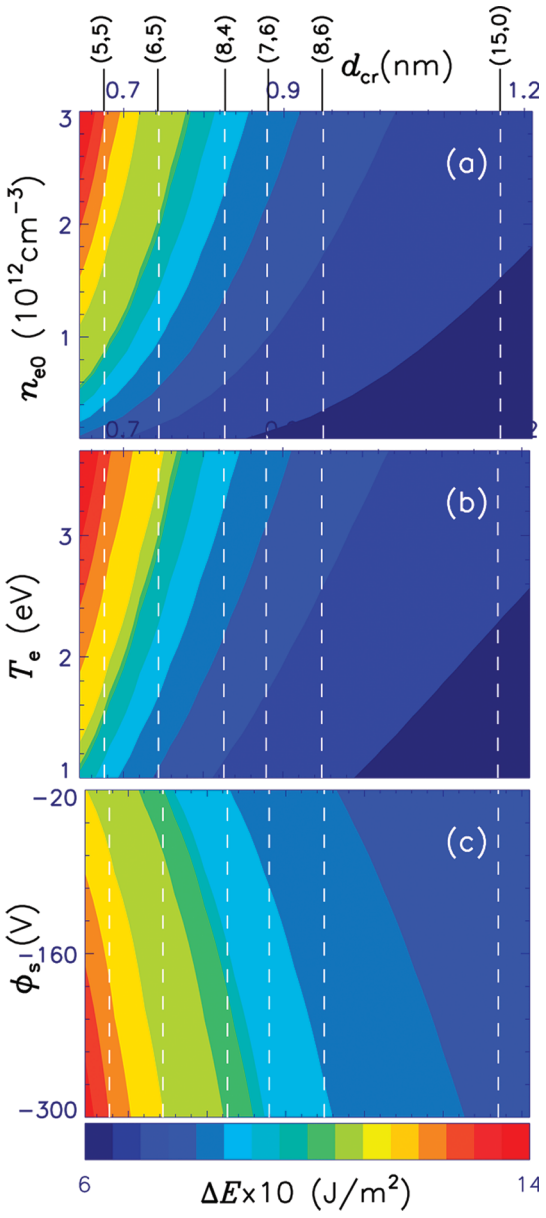

Figure 4. Link in a 3D parameter space between the plasma parameters ((a) plasma density n_{e0}; (b) electron temperature T_e; and (c) surface potential Φ_S), critical diameter d_{cr}, and bending energy ΔE (multiplied by a factor of 10) in the plasma-based SWCNT growth. Unless varied in any particular plot, the default set of parameters is T_e = 1.0 eV, T_i = 0.05 eV, $n_{e0} = 5.0 \times 10^{11}$ cm^{-3}, P_0 = 50 mTorr, $\Phi_S = -100$ V, r_{Ar} = 70%, r_{CH} = 20%, and r_H = 10%. Examples of (6,5),[6,10] (8,4),[6,10] (7,6),[6,9−11] and (8,6)[11] semiconducting and (5,5) and (15,0) metallic nanotubes are shown. The graded-color contour plots (a) and (b) correspond to T_H = 650 °C, while plot (c) has T_H = 750 °C.

produce up to 96% of thin semiconducting SWCNTs in the plasma.[9−11] On the other hand, in thermal CVD, which has to be operated at higher substrate temperatures, not only thicker nanotubes but also a broader size distribution, as well as a larger abundance of metallic nanotubes compared to the plasma-based growth, are expected.[9,33]

However, one should exercise caution using very small catalyst nanoparticles (*e.g.*, smaller than 1 nm) as the smaller size and the increased carbon solubility may easily lead to catalyst poisoning due to overfeeding.[35] It is thus imperative to properly balance the rates of carbon delivery to the surface and removal of excess material from the surface. In the plasma it can be achieved by faster delivery of carbon atoms to the catalyst while simultaneously etching amorphous carbon away.[17,20,28] On the other hand, using catalyst nanoparticles above a certain size results in larger nucleation thresholds, much larger critical nuclei, and low bending energy (per area), eventually leading to nanocage-like structures.[24]

Size/Chirality Selectivity and Experimental Support. To further explain the experimental reports on the effective SWCNT chirality control in the plasma, we have linked the plasma-specific parameters (the electron temperature T_e, the plasma density at the plasma−sheath boundary n_{e0}, and the substrate potential Φ_S), the GL critical diameter d_{cr}, and the bending energy ΔE. The results are plotted in Figure 4 using a three-dimensional graded-color contour plot for ΔE. The range of GL critical diameters (which in turn determines possible SWCNT chiralities) was chosen to cover the nanotube sizes achieved in the recent plasma-based experiments. We have selected four semiconducting SWCNTs (of chirality of (6,5), (8,4),[6,9,10] (7,6),[6,9,11,10] and (8,6)[11]) and two armchair (5,5) and zigzag (15,0) metallic nanotubes, in line with the expected 2:1 "natural" abundance ratio. Using the graded-color contour plots, we have identified the most probable combinations of the catalyst nanoparticle sizes and plasma-based process parameters to enhance the nucleation of the selected nanotubes. For example, the nucleation probability of a 0.74 nm thick (5,5) metallic SWCNT becomes higher with the increasing electron temperature T_e, plasma density n_{e0}, and the magnitude of the (negative) surface potential with respect to the plasma bulk Φ_S. This can be explained by noting that all these changes (in T_e, n_{e0}, and Φ_S) lead to higher ion energies upon impact on the CNP surface. This leads to more effective carbon production *via* ion-induced dissociation of precursor species on the catalyst surface. The surface heating also becomes more effective through larger amounts of energy released through the plasma−surface interactions. Consequently, the catalyst becomes hotter, and the number of carbon atoms on its surface increases. As a result, the bending energy also increases, giving rise to stable, small graphene nuclei. In turn, this favors the formation of very thin SWCNTs with a narrow thickness/chirality distribution. In other words, additional plasma heating facilitates nucleation of thin SWCNTs at relatively low substrate holder (external heating) temperatures. This conclusion is consistent with the experimental measurements of the SWCNT diameter distributions of thin SWCNTs produced in low-temperature plasmas.[10−12]

The pronounced increase of the bending energy with the plasma density for very small critical nuclei in Figure 4a explains the recent experimental observation of a strong shift toward smaller diameters and a broader spectrum of semiconducting nanotubes as the plasma density increases.[11] Moreover, the results in Figure 4a also suggest that for thinner nanotubes the increase in the bending energy with the plasma density is much steeper than for thicker ones. Hence, the probability of nucleation of the thinner tubes becomes relatively higher, which in turn leads to narrower chirality distributions in denser plasmas. These results also explain the recent experimental observation that an increase of the rf discharge power (and hence, the plasma density) led to the narrower nanotube chirality distribution.[10] It is noteworthy that this effect was very clearly observed in the experiment when the power was increased above a certain threshold. In other words, the plasma density should not be too low to lead to the better size/chirality selectivity of thin SWCNTs. This is also supported by the results in Figure 4a, where one can clearly see that the difference between the bending energies becomes notably larger as the plasma density increases.

The results in Figure 4 also explain the experimental trends related to the variations in the plasma sheath width and hydrocarbon precursor supply.[10] It was reported that when the sheath width/potential difference were large, the high hydrocarbon supply conditions prevailed. Under such conditions the nanotube size/chirality distributions were narrow; otherwise, under low hydrocarbon supply conditions this distribution was broad. From Figure 4c it follows that as the surface potential (with respect to the plasma bulk) increases, the rate of supply of carbon precursors (BUs) increases. This increase is accompanied by an increase in the bending energy, which becomes even steeper as the nanotube size decreases. Therefore, the probability of nucleation of thinner nanotubes increases, which explains the experimentally observed narrow size distributions under narrow plasma sheath conditions. The changes in the sheath width and hydrocarbon supply in the experiments[10] may also be caused by higher electron temperatures, which in addition to the stronger increase of the bending energy for thinner nanotubes (Figure 4b) also lead to higher ionization and dissociation rates. As a result, the rates of carbon supply to the catalyst nanoparticles also increase.

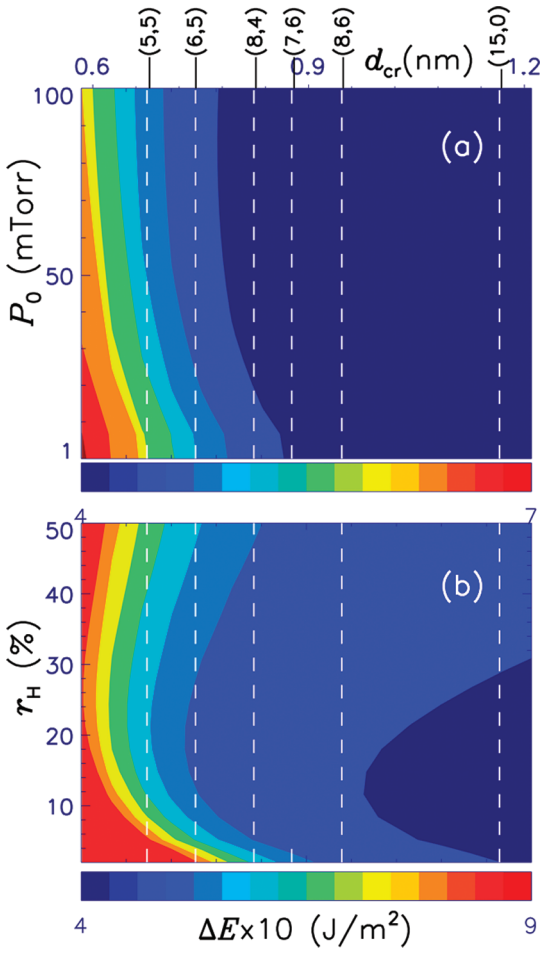

Figure 5. Link in a 3D parameter space between the parameters of the precursor gas mixture ((a) total pressure P_0; (b) relative abundance of hydrogen gas r_H), critical diameter d_{cr}, and bending energy ΔE (multiplied by a factor of 10) in the plasma-based SWCNT growth. Unless varied in any particular plot, the default set of parameters is T_e = 1.0 eV, T_i = 0.05 eV, $n_{e0} = 5.0 \times 10^{11}$ cm^{-3}, P_0 = 50 mTorr, $\Phi_S = -100$ V, r_{Ar} = 70%, r_{CH} = 20%, r_H = 10%, and T_H = 500 °C. The SWCNT examples are the same as in Figure 4.

It was also reported that the selectivity in the nanotube size and metallicity can be substantially increased when the process temperatures decrease.[9,10] Indeed, the yield of semiconducting nanotubes in the array can be as high as 96% under low-temperature plasma synthesis conditions.[9] The better size selectivity of smaller nanotubes at low temperatures is confirmed by the results in Figure 2b,c and Figure 3b,c, which suggest a larger difference in the sizes of critical nuclei and the bending energies between the nanotubes of different sizes under such conditions. This can also be understood by noting that when a temperature is high, carbon atoms in the as-formed nucleus are more mobile and a larger number of nuclei with different sizes can be bent and form nanotube structures.

There is recent experimental evidence that the selectivity of thin SWCNT growth at low temperatures is strongly affected by the operating pressure and percentage of hydrogen in the gas mixture.[10,12,32] To explain these observations, in Figure 5 we present a similar 3D contour plot where the total gas pressure P_0 and percentage of hydrogen in the gas mixture r_H are used instead of the plasma-related parameters used in Figure 4.

As Figure 5a shows, the GL bending energy increases with decreasing the total gas pressure. This is a strong indicator of the growth of thinner SWCNTs at low gas pressures, as a result of nucleation of stable small-diameter graphene layers on the catalyst nanoparticles, which was also confirmed experimentally.[9,32] This can be explained by noting that the plasma sheath becomes wider at lower pressures. In this case the sheath width increases, leading to stronger hydrocarbon precursor fluxes onto the catalyst nanoparticle surface. More energetic ions reach the substrate, thus enhancing ion-induced precursor dissociation. This in turn leads to the higher bending energy and more likely nanotube nucleation.

An interesting feature observable from Figure 5b is a nonmonotonic trend in the dependence of the GL bending energy on the hydrogen gas ratio r_H. Below $r_H \approx 25\%$ the tendency is decreasing and reverses afterward. This change is the strongest in the range of nanotube diameters below 0.8 nm, which is particularly important in applications that rely on quantum size effects. This can be explained by the interplay of the species delivery and surface heating effects. When the percentage of hydrogen increases from small amounts toward ~20%, the bending energy decreases, which is likely due to effective recombination of carbon and hydrogen atoms. This recombination reduces the amount of carbon atoms that can be extruded to the surface, and hence, the bending energy is expected to decrease, as shown in Figure 5b. With a further increase of r_H, the catalyst heating induced by the plasma–surface interactions (*e.g.*, hydrogen recombination and ion impact processes shown in Figure 1c) prevails over the carbon atom loss due to recombination. These processes make the surface hotter, thereby increasing the rates of thermal dissociation of hydrocarbon precursors. As a result, the carbon concentration in the AuC alloy ζ increases, which eventually reverses the decreasing trend in the dependence of ΔE on r_H. Importantly, this trend reversal is particularly strong for very thin SWCNTs. Therefore, variation of hydrogen content turns out to be one of the most effective controls in nucleation and chirality selectivity of thin single-walled carbon nanotubes. This result is consistent with the experimentally reported decrease of the SWCNT diameters and also narrower chirality distributions of SWCNTs after the hydrogen gas pressure is increased in the reactive plasmas of $C_xH_y + H_2$ gas mixtures.[12,32] It is also relevant to note that in the plasma one can achieve highly controlled production of specific reactive species,[36] such as carbon atoms C or

dimers C_2, which show two different reaction paths to change SWCNT chirality through low-threshold incorporation into the developing carbon nanotube caps.[37] This offers additional opportunities for the effective control of SWCNT chirality.

However, our calculations cannot directly explain the so dramatic increases of the abundance of semiconducting nanotubes in the plasma reported experimentally.[9,10] However, this increase is the strongest in the low-pressure range, when thinner nanotubes become better identifiable (*e.g.*, by stronger photoluminescence excitation (PLE) signals and better-contrast 3D (diameter-wavelength-intensity) PLE maps) at lower temperatures. This is consistent with our calculations in Figure 4 and Figure 5 if one assumes that among the most commonly observed nanotubes, the average thickness of the metallic nanotubes is larger compared to semiconducting ones. The results of our calculations in Figure 5a also suggest that higher plasma density (and, hence, the increased hydrocarbon precursor supply) significantly increases the bending energy of the (5,5) and (15,0) metallic nanotubes. This is consistent with the experimental observation[9] that larger hydrocarbon supply leads to larger fractions of metallic nanotubes. This point should be explored in greater detail by taking into account microscopic details of the nanotube nucleation on CNPs of specific sizes.

This also prompts us to discuss the possible role of catalyst material in the nucleation of SWCNTs in the plasma. It was reported that the ratio of intensities of D and G peaks in Raman spectra, I_D/I_G (which is the measure of the relative presence of SWCNTs in the array), did not change significantly when Au and Fe catalysts were used.[12] This suggests the importance of the process-related factors (precursors, temperature, biasing conditions, pressure, *etc.*) in the SWCNT nucleation and growth. However, catalyst nanoparticles made of different materials show quite different responses to the changes in the process conditions. For example, SWCNTs grown on a Fe catalyst do not show any clear dependence on the hydrogen flow rate, while this dependence is very strong in the Au catalyst case.[12]

Another interesting experimental fact is that the SWCNT diameters are larger for Fe catalyst nanoparticles compared to Au.[12] Since the energies for C−Fe bonds are larger compared to C−Au bonds,[38,39] one can expect intrinsically larger bending energies for Au catalysts under the same conditions. Our results in Figure 3 suggest that smaller graphene nuclei also tend to bend better in the plasma. Thus, thinner SWCNTs are expected on Au nanoparticles. To cement this conclusion, we have also shown that the relative gains due to the GT effect δ_P^{GT} (Figure 3c) for Au catalyst nanoparticles are larger compared to Fe CNPs of the same size under the same plasma process conditions. This happens because the driving force for the nucleation of GL on a gold CNP, $\Delta\mu_{ls}^{Au}$, is larger than the corresponding driving force, $\Delta\mu_{ls}^{Fe}$, for iron catalyst. This is why the associated increase in the bending energy ΔE in Au nanoparticles is due not only to the lower work of adsorption W_{ad} but also, as our calculations suggest, to a stronger GT effect, which in turn leads to larger kinetic energy, E_K, of carbon atoms.

To conclude this section, we emphasize that a combination of numerical results representative of typical conditions of the plasma-based SWCNT synthesis suggests a simple practical approach to maximize the benefits of the process-related conditions to achieve the as-yet elusive nanotube growth with a high (ultimately deterministic) selectivity between the abundance of different nanotube chiralities and conductivity types in an array. This is particularly important compared to the approaches based on catalyst tailoring since it is much easier and less time-, effort-, and cost-consuming to adjust process conditions rather than deliberately tailoring catalyst layers and arrays, which usually require several additional process steps carried externally to the main nanotube growth reactor. The graphs in Figures 2 and 3 and 3D maps in Figure 4 and 5 allow one to select the most appropriate Au catalyst nanoparticle sizes, precursor gas composition, working pressure, substrate temperature, and plasma parameters to predict more effective nucleation of SWCNTs with any specific size/chirality distribution or otherwise produce other carbon nanostructures such as nanocages or small graphene nanodots.

CONCLUSIONS

Our numerical results therefore explain and quantify the common experimental observations of the possibility of the narrow diameter/chirality distribution of SWCNT grown in low-temperature plasma experiments,[9−13] where the catalyst structures (which also turn out to be critical in the chirality-selective nanotubes growth[6]) can be preserved from unwanted deformation, coagulation, *etc.*, which are usual artifacts of high-temperature CVD processes.[40]

We have also shown that the differences between the nucleation barriers, critical nuclei, and bending energies for different Au CNP radii in PECVD are notably larger than in thermal CVD, thus leading to the better size selectivity in a broader size range of catalyst nanoparticles used. We have also presented the results of detailed investigations of the effects of the main plasma process parameters on the GL bending energy, showing how variations in the plasma parameters may lead to effective control of the SWCNT nucleation.

One of the main outcomes of this work is that the "evil" Gibbs−Thomson effect, which makes thin nanotube nucleation in thermal CVD much harder, can be gainfully used in the plasma-based process, which not only minimizes the negative impact of the GT effect (higher nucleation barriers) but also dramatically enhances its positive impact on the graphene layer bending.

As the plasma effects get stronger, so does the GT effect, which suggests the possibility of a truly constructive interplay between these two seemingly unrelated effects in producing thin single-walled carbon nanotubes with narrow size and chirality distributions at low process temperatures, using small catalyst nanoparticles.

Our study is the first systematic numerical study of the recent experimental breakthroughs in the possibility of effective control of SWCNT chirality distributions using low-temperature plasmas and explains a host of relevant experimental observations. It can also be used to further improve the predictability of (not only plasma-based) carbon nanostructure synthesis experiments and approach the ultimate goal of energy-efficient, cost-effective, environment-friendly deterministic nanofabrication.

METHODS

Overview and Main Assumptions. We consider the Au CNP-assisted nucleation of a SWCNT in reactive plasmas of Ar + H_2 + CH_4 gas mixtures commonly used in plasma-aided synthesis of CNTs.[17,20] The combinatorial, multiphase, multiscale model includes the plasma sheath, ion/radical transport, species creation/loss, plasma–surface interaction, heat transfer, surface/bulk diffusion, graphene layer nucleation, and bending/lift-off modules. Figure 1 shows the schematics of the key neutral and ionic species (a), plasma sheath (b), magnified sketch of the Au CNP, key-species deposition, and prevailing plasma-induced processes (such as surface and bulk diffusion of C species, hydrogen atom recombination, and ion neutralization) on the CNP surface (c), and the GL nucleation on the Au CNP (d) predeposited on a conducting substrate of thickness d placed on a substrate holder, which is heated externally to temperature T_H. The BUs are created on the surface of the hemispheric Au catalyst *via* ion decomposition and ion-assisted and thermal dissociation processes. The first two processes are dominant at low temperatures and become more effective as the ion energy and fluxes onto the surface increase. The latter process is more effective when the catalyst temperature rises due to the external and plasma heating. Carbon atoms diffuse into the catalyst *via* its bulk and through its surface (SD and BD processes as sketched in Figure 1c).

Here, it is assumed that the surface precipitation (and saturation) time is much shorter than the bulk diffusion time, due to relatively high precursor pressures used. In this case the SWCNT growth proceeds in the base-led mode.[41] Higher concentration of carbon atoms in the catalyst AuC alloy increases the concentration of carbon atoms on the CNP surface, which is favorable for GL nucleation. Meanwhile, the energy released *via* plasma-induced reactions (such as hydrogen atom recombination, ion neutralization, and collisions of species with the catalyst surface) makes the CNP hotter,[42,43] giving rise to more effective thermal dissociation of the neutral hydrocarbons; thus more carbon atoms are created, diffuse, and then (after saturating the AuC alloy) precipitate on the top surface of the CNP, where the graphene layer nucleates.

Plasma Sheath, Ion/Radical Transport, Species Creation/Loss, Plasma–Surface Interaction, and Heat Transfer Modules. Here we account for the adsorption and desorption of species, the thermal and ion-induced dissociation of hydrocarbon species on the CNP surface, carbon atom evaporation, and all ion–surface collisions.[42] The heating model accounts for the energies released or taken *via* these surface processes[44] as well as through hydrogen atom recombination and hydrogen ion neutralization on the catalyst surface. The carbon atom production module includes the mass balance equation for carbon atoms

$$J_C^+ + D_s \frac{1}{r_C^2 \sin\theta} \frac{d}{d\theta}\left(\sin\theta \frac{d\hat{n}_C}{d\theta}\right) - J_C^- = 0 \qquad (1)$$

on the catalyst nanoparticle surface as well as similar equations for other key species, which can be obtained from eq 1 by appropriate replacement of subscripts denoting the species.[42,44] In eq 1, the first term, J^+_C, describes the creation of carbon atoms on the Au CNP surface due to thermal and ion-induced dissociation of hydrocarbon radicals and ions. The second term in eq 1 accounts for the carbon atom loss due to surface diffusion, whereas the third term describes carbon atom loss due to evaporation, interaction of carbon species with atomic hydrogen, and carbon diffusion into the bulk of the Au CNP. Here, n_C is the surface density of carbon atoms produced, D_s is the surface diffusion coefficient, and r_C is the CNP radius.

The plasma-sheath model equations relate the sheath thickness, λ_s, and ion energies to the plasma-specific parameters such as the electron temperature T_e, plasma density n_e, and substrate potential. These equations were used to calculate kinetic ion energies and fluxes of the ion species to the substrate, which are required in the species production module (*e.g.*, eq 1). The energy balance equation (complemented with boundary conditions in the heat transfer module) in turn describes the temperature distribution along the Si substrate, which is used to determine the catalyst nanoparticle temperature T_D and its difference from the substrate holder temperature T_H; the latter can be quite substantial in PECVD experiments, in some cases reaching ~100 °C and even higher.[45]

Surface/Bulk Diffusion, Graphene Layer Nucleation, and Bending/Lift-off Modules. Using the output from the above modules, one can calculate the catalyst temperature-dependent fluxes of carbon atoms through the catalyst bulk,

$$J_v = \int_0^{\pi/2} (\pi \hat{n}_C D_b / A_d) 2\pi r_C^2 \sin\theta \, d\theta$$

and the catalyst surface

$$J_s = -2\pi (D_s \, d\hat{n}_C/d\theta)|_{\theta = 90^\circ}$$

and their diffusion into the catalyst through the border ($\theta = 90°$), where $A_d = 2\pi r_C^2$ is the surface area of the hemisphere CNP exposed to the plasma.

After the saturation of the liquid alloy in the CNP, carbon atoms are extruded from the CNP and then react on the surface, leading to the formation of a continuous graphene layer with the height $h = 0.34$ nm on the CNP surface.[45] It is assumed that during the GL nucleation stage the CNP radius does not change. The concentration of the carbon atoms in the AuC alloy ζ can be obtained from the kinetic equation of CNT growth in the monolayer nucleation approximation, with the Gibbs–Thomson effect being taken into account.[19] The kinetic growth equation relates the bulk J_v and surface J_s diffusion fluxes of carbon atoms (obtained from the species creation/loss module) to the carbon incorporation and desorption fluxes. The minimum energy (energy barrier) ΔG_N^* required for the nucleation is obtained by maximizing the Gibbs free energy of monolayer graphene formation.[46] The critical diameter of the graphene layer,

$$d_{cr} = 2 B r_C / (A^2 + B^2)^{1/2}$$

is obtained by maximizing the Gibbs free energy, where

$$A = 2\pi r_C [-h \Delta_l \mu^{GT}{}_{sl}/\Omega + \gamma_{GV} + \gamma_{GS} - \gamma_{SV}]$$

and

$$B = 2\pi [\varepsilon + 2Q_C/9h]$$

Here, Ω is the molar volume, ε is the specific edge energy, and γ_{GV}, γ_{GS}, and γ_{SV} are the interfacial surface energies of

the GL−vapor, GL−Au, and Au−vapor interfaces, respectively. In this work, Q_C = 4.4 eV[47] is used to account for the strain energy that originates from the bending of the graphene layer when the edge-atom orbitals overlap with those of surface Au atoms.[46] Furthermore, $\Delta\mu^{GT}_{sl}$ is the size-dependent difference in chemical potentials in the liquid and solid phases, which is reduced as the GT effect becomes stronger at smaller r_C. Finally, the bending energy ΔE is defined as the difference between the kinetic energy of carbon atoms, E_K, and the work of adhesion, W_{Ad}, per unit surface area of the graphene layer.[23] The energy barrier for GL nucleation, ΔG_N^*, and the critical diameter, d_{cr}, decrease if the carbon concentration, ζ, increases, while E_K increases. This makes the formation of the stable, very small GL more likely to happen, which is favorable for the nucleation and growth of thin SWCNTs with good diameter/chirality selectivity.

It is also worthwhile to mention that the size of the critical nucleus (which is intimately related to the size of the catalyst nanoparticle) is one of the most important factors that determines the nanotube chirality. However, this simple factor does not fully account for the interactions between the nanotube nucleus and the catalyst nanoparticles, which involves step edges, crystalline planes, and dislocations on the surface.[7,48,49] These interactions prevent the as-formed nucleus from further expansion over the catalyst surface and facilitate the lift-off process through additional stress at the edge of the graphene nucleus. Accounting for these fine structural factors requires more sophisticated atomistic models.

Another known manifestation of the Gibbs−Thomson effect is the reduction of the melting temperature of catalyst nanoparticles due to the curvature of the solid−liquid interface.[50,51] Since the exact melting points of nanoparticles are size-dependent and in most cases are not known, reliable knowledge of the GT coefficients appears to be very useful to predict the activation energies and optimum growth temperatures for single-walled nanotubes of different chiralities.

Acknowledgment. This work was partially supported by the Australian Research Council and CSIRO's OCE Science Leadership Program.

Supporting Information Available: Main equations of the model and the description of calculation procedures, additional results on the effects of variations of the plasma-specific parameters on the bending energy, and their relevance to the experimental results. This material is available free of charge *via* the Internet at http://pubs.acs.org.

REFERENCES AND NOTES

1. Iijima, S.; Ichihashi, T. Single-Shell Carbon Nanotubes of 1-nm Diameter. *Nature* **1993**, *363*, 603–605.
2. Baughman, R. H.; Zakhidov, A. A.; De Heer, W. A. Carbon Nanotubes: The Route Toward Applications. *Science* **2002**, *297*, 787–792.
3. Javey, A.; Guo, J.; Wang, Q.; Lundstrom, M.; Dai, H. Ballistic Carbon Nanotube Field-Effect Transistors. *Nature* **2003**, *424*, 654–657.
4. Meyyappan, M., Ed. *Carbon Nanotubes: Science and Applications*; CRC Press: Boca Raton, FL, 2004.
5. Liu, H.; Nishide, D.; Tanaka, T.; Kataura, H. Large-Scale Single-Chirality Separation of Single-Wall Carbon Nanotubes by Simple Gel Chromatography. *Nat. Commun.* **2011**, *2*, 309−317. DOI: 10.1038/ncomms1313.
6. Chiang, W.-H.; Sankaran, R. M. Linking Catalyst Composition to Chirality Distributions of As-Grown Single-Walled Carbon Nanotubes by Tuning Ni_xFe_{1-x} Nanoparticles. *Nat. Mater.* **2009**, *8*, 882–886.
7. Ding, F.; Harutyunyan, A.; Yakobson, B. Dislocation Theory of Chirality-Controlled Nanotube Growth. *Proc. Natl. Acad. Sci. U. S. A.* **2009**, *106*, 2506–2509.
8. Neyts, E. C.; Shibuta, Y.; van Duin, A. C. T.; Bogaerts, A. Catalyzed Growth of Carbon Nanotube with Definable Chirality by Hybrid Molecular Dynamics - Force Biased Monte Carlo Simulations. *ACS Nano* **2010**, *4*, 6665–6672.
9. Qu, L.; Du, F.; Dai, L. Preferential Synthesis of Semiconducting Vertically Aligned Single-Walled Carbon Nanotubes for Direct Use in FETs. *Nano Lett.* **2008**, *8*, 2682–2687.
10. Kato, T.; Hatakeyama, R. Direct Growth of Short Single-Walled Carbon Nanotubes with Narrow-Chirality Distribution by Time-Programmed Plasma Chemical Vapor Deposition. *ACS Nano* **2010**, *4*, 7395–7400.
11. Volotskova, O.; Fagan, J. A.; Huh, J. Y.; Phelan, F. R.; Shashurin, A.; Keidar, M. Tailored Distribution of Single-Wall Carbon Nanotubes from Arc Plasma Synthesis Using Magnetic Fields. *ACS Nano* **2010**, *4*, 5187–5192.
12. Ghorannevis, Z.; Kato, T.; Kaneko, T.; Hatakeyama, R. Narrow-Chirality Distributed Single-Walled Carbon Nanotube Growth from Nonmagnetic Catalyst. *J. Am. Chem. Soc.* **2010**, *132*, 9570–9572.
13. Hatakeyama, R.; Kaneko, T.; Kato, T.; Li, Y. F. Plasma-Synthesized Single-Walled Carbon Nanotubes and their Applications. *J. Phys. D.: Appl. Phys.* **2011**, *44*, 174004.
14. Sankaran, R. M. Towards Chirality-Controlled SWCNTs: Can a Plasma Help? *J Phys. D.: Appl. Phys.* **2011**, *44*, 174005.
15. Keidar, M. Factors Affecting Synthesis of Single Wall Carbon Nanotubes in Arc Discharge. *J. Phys. D: Appl. Phys.* **2007**, *40*, 2388–2393.
16. Neyts, E. C.; Shibuta, Y.; Bogaerts, A. Bond Switching Regimes in Nickel and Nickel-Carbon Nanoclusters. *Chem. Phys. Lett.* **2010**, *488*, 202–205.
17. Ostrikov, K. Colloquium: Reactive Plasmas as a Versatile Nanofabrication Tool. *Rev. Mod. Phys.* **2005**, *77*, 489–511.
18. Dubrovskii, V. G.; Cirlin, G. E.; Soshnikov, I. P.; Tonkikh, A. A.; Sibirev, N. V.; Samsonenko, Yu. B.; Ustinov, V. M. Diffusion-Induced Growth of GaAs Nanowhiskers During Molecular Beam Epitaxy: Theory and Experiment. *Phys. Rev. B.: Condens. Matter Mater. Phys.* **2005**, *71*, 205325–205330.
19. Ostrikov, K.; Mehdipour, H. Rapid, Simultaneous Activation of Thin Nanowire Growth in Low-Temperature, Low-Pressure Chemically Active Plasmas. *J. Mater. Chem.* **2011**, *21*, 8183–8191.
20. Meyyappan, M. A Review of Plasma Enhanced Chemical Vapor Deposition of Carbon Nanotubes. *J. Phys. D: Appl. Phys.* **2009**, *42*, 213001.
21. Ding, F.; Bolton, K.; Rosen, A. Nucleation and Growth of Single-Walled Carbon Nanotubes: A Molecular Dynamics Study. *J. Phys. Chem. B* **2004**, *108*, 17369–17377.
22. Miyauchi, Y.; Chiashi, S.; Murakami, Y.; Hayashida, Y.; Maruyama, S. Fluorescence Spectoroscopy of Single-Walled Carbon Nanotubes Synthesized Alcohol. *Chem. Phys. Lett.* **2004**, *387*, 198–203.
23. Kanzow, H.; Lenski, C.; Ding, A. Single-Wall Carbon Nanotube Diameter Distributions Calculated from Experimental Parameters. *Phys. Rev. B: Condens. Matter Mater. Phys.* **2001**, *63*, 125402–125407.
24. Lin, M.; Tan, J. P. Y.; Boothroyd, C.; Loh, K. P.; Tok, E. S.; Foo, Y. -L. Direct Observation of Single-Walled Carbon Nanotube Growth at the Atomistic Scale. *Nano Lett.* **2006**, *6*, 449–452.
25. Lu, C.; Liu, J. Controlling the Diameter of Corbon Nanotube in Chemical Vapor Deposition Method by Carbon Feeding. *J. Phys. Chem. B* **2006**, *110*, 20254–20257.
26. Louchev, O. A.; Laude, T.; Sato, Y.; Kanda, H. Diffusion-Controlled Kinetics of Carbon Nanotube Forest Growth by Chemical Vapor Deposition. *J. Chem. Phys.* **2003**, *118*, 7622–7634.
27. Denysenko, I; Ostrikov, K. Ion-Assisted Precursor Dissociation and Surface Diffusion: Enabling Rapid, Low-Temperature Growth of Carbon Nanofibers. *Appl. Phys. Lett.* **2007**, *90*, 251501–251503.
28. Ostrikov, K.; Levchenko, I.; Cvelbar, U.; Sunkara, M.; Mozetic., M. Form Nucleation to Nanowires: A Single-Step Process in Reactive Plasmas. *Nanoscale* **2010**, *2*, 2012–2027.
29. Thess, A.; Lee, R.; Nikolaev, P.; Dai, H.; Petit, P.; Robert, J.; Xu, C.; Lee, Y. H.; Kim, S. G.; Rinzler, A. G.; *et al.* Crystalline Ropes of Metallic Carbon Nanotubes. *Science* **1996**, *273*, 483–487.
30. Kanzow, H.; Schmalz, A.; Ding, A. Laser-Assisted Production of Multi-Walled Carbon Nanotubes from Acetylene. *Chem. Phys. Lett.* **1998**, *295*, 525–530.

31. Hernadi, K.; Fonseca, A.; Nagy, J. B.; Bernaerts, D.; Lucas, A. A. Fe-Catalyzed Carbon Nanotube Formation. *Carbon* **1996**, *34*, 1249–1257.
32. Kato, T.; Hatakeyama, R. Diameter Tuning of Single-Walled Carbon Nanotubes by Diffusion Plasma CVD. *J. Nanomater.* **2010**, *2011*, 490529.
33. Li, Y.; Mann, D.; Rolandi, M.; Kim, W.; Ural, A.; Hung, S.; Javey, A.; Cao, J.; Wang, D.; Yenilmez, E.; *et al*. Preferential Growth of Semiconducting Single-Walled Carbon Nanotubes by a Plasma Enhanced CVD Method. *Nano Lett.* **2004**, *4*, 317–321.
34. Robertson, J.; Zhong, G.; Telg, H.; Thomsen, C.; Warner, J. H.; Briggs, G. A. D.; Dettlaff-Weglikowska, U.; Roth, S. Growth and Characterization of High-Density Mats of Single-Walled Carbon Nanotubes for Interconnects. *Appl. Phys. Lett.* **2008**, *93*, 163111–163113.
35. Zhou, W.; Ding, L.; Liu, J. Role of Catalysts in the Surface Synthesis of Single-Walled Carbon Nanotubes. *Nano Res.* **2009**, *2*, 593–598.
36. Ostrikov, K.; Yoon, H. J.; Rider, A.; Vladimirov, S. V. Two-Dimensional Simulation of Nanoassembly Precursor Species in $Ar+H_2+C_2H_2$ Reactive Plasmas. *Plasma Proc. Polym.* **2007**, *4*, 27–40.
37. Wang, Q.; Ng, M.-F.; Yang, S.-W.; Yang, Y.; Chen, Y. Carbon Nanotube Growth and Chirality Selection Induced by Carbon Atom and Dimer Addition. *ACS Nano* **2010**, *4*, 939–946.
38. Ding, F.; Larsson, P.; Larsson, J. A.; Ahuja, R.; Duan, H.; Rosen, A.; Bolton, K. The Importance of Strong Carbon-Metal Adhesion for Catalytic Nucleation of Single-Walled Carbon Nanotubes. *Nano Lett.* **2008**, *8*, 463–468.
39. Sun, C. Q. Size Dependence of Nanostructures: Impact of Bond Order Deficiency. *Prog. Solid State Chem.* **2007**, *35*, 1–159.
40. Naumov, A.; Kunestov, O. A.; Harutyunyan, A. R.; Green, A. A.; Hersam, M. C.; Resasco, D. E.; Nikolaev, P. N.; Weisman, R. B. Quantifying the Semiconducting Fraction in Single-Walled Carbon Nanotube Sample Through Comparative Atomic Force and Photoluminescence Microscopy. *Nano Lett.* **2009**, *9*, 3203–3208.
41. Melechko, A. V.; Merkulov, V. I.; Lowndes, D. H.; Guillorn, M. A.; Simpson, M. L. Transition Between `Base' and `Tip' Carbon Nanofiber Growth Modes. *Chem. Phys. Lett.* **2002**, *356*, 527–533.
42. Mehdipour, H.; Ostrikov, K.; Rider, A. E. Low- and High-Temperature Controls in Carbon Nanofiber Growth in Reactive Plasma. *Nanotechnology* **2010**, *21*, 455605.
43. Wolter, M.; Levchenko, I.; Kersten, H. Hydrogen in Plasma-Nano-Fabrication: Selective Control of Nanostructure Heating and Passivation. *Appl. Phys. Lett.* **2010**, *96*, 133105–133107.
44. Denysenko, I.; Ostrikov, K. Plasma Heating Effects in Catalyzed Growth of Carbon Nanofibers. *J. Phys. D: Appl. Phys.* **2009**, *42*, 015208.
45. Meyyappan, M.; Delzeit, L.; Cassell, A.; Hash, D. Carbon Nanotube Growth by PECVD: a Review. *Plasma Sources Sci. Technol.* **2003**, *12*, 205.
46. Kuznetsov, V. L.; Usoltseva, A. N.; Chuvilin, A. L. Thermodynamic Analysis of Nucleation of Carbon Deposit on Metal Particles and its Implications for the Growth of Carbon Nanotubes. *Phys. Rev. B: Condens. Matter Mater. Phys.* **2001**, *64*, 235401–235407.
47. Tomanek, D.; Zhong, W.; Krastev, E. Stability of Multishell Fullerenes. *Phys. Rev. B* **1993**, *48*, 15461–15464.
48. Zhu, H.; Suenaga, K.; Wei, J.; Wang, K.; Wu, D. A Strategy to Control the Chirality of Single-Walled Carbon Nanotubes. *J. Cryst. Growth* **2008**, *310*, 5473–5476.
49. Koziol, K. K. K.; Ducati, C.; Windle, A. H. Carbon Nanotubes with Catalyst Controlled Chiral Angle. *Chem. Mater.* **2010**, *22*, 4904–4911.
50. Shibuta, Y.; Suzuki, T. A. Molecular Dynamics Study of the Phase Transition in bcc Metal Nanoparticles. *J. Chem. Phys.* **2008**, *129*, 144102.
51. Shiozawa, H.; Kramberger, C.; Pfeiffer, R.; Kuzmany, H.; Pichler, T.; Liu, Z.; Suenaga, K.; Kataura, H.; Silva, S. R. P. Catalyst and Chirality Dependent Growth of Carbon Nanotubes Determined Through Nano-Test Tube Chemistry. *Adv. Mater.* **2010**, *22*, 3685–3689.